Ultrathin mono-resonant nano photovoltaic device for broadband solar conversion

Florian Proise, Anne-Laure Joudrier, Fabrice Pardo, Jean-Luc Pelouard, Jean-Francois Guillemoles

Research Article | Vol. 26, No. 18 | 3 Sep 2018 | OPTICS EXPRESS A806

Optics EXPRESS

Ultrathin mono-resonant nano photovoltaic device for broadband solar conversion

FLORIAN PROISE,[1,2] ANNE-LAURE JOUDRIER,[3] FABRICE PARDO,[2] JEAN-LUC PELOUARD,[2] AND JEAN-FRANÇOIS GUILLEMOLES[1,*]

[1]*CNRS, Institut Photovoltaïque d'Ile-de-France IPVF - UMR 9006, 30 route Départementale 128, 91120 Palaiseau, France*
[2]*CNRS, Centre de Nanosciences et Nanotechnologies C2N, Route de Nozay, 91460 Marcoussis, France*
[3]*ENSCP Chimie-Paristech, Institut Photovoltaïque d'Ile-de-France IPVF - UMR 9006, 30 route Départementale 128, 91120 Palaiseau, France*
jf.guillemoles@chimieparistech.psl.eu

Abstract: Nano-resonators can be used in photovoltaics to drastically improve the ability of the device to absorb light and generate photo-carriers, therefore enabling a reduction of the absorber volume. Conventionally, the harvest of the spectrally broad solar spectrum is achieved via the tedious engineering of multiple optical resonances. In this paper, we propose a breakthrough approach, which consists in reducing the solar spectral range with a spectral conversion layer to match only one resonance that can then be easily designed. We use a Maxwell solver and a ray-tracing code to optimize the nano-resonator and its spectral converter. We show that 66.2% optical efficiency can be theoretically achieved in less than 40 nm mean thick absorber while leading to device design enabling collection of photo-generated carriers.

OCIS codes: (040.5350) Photovoltaic; (050.6624) Subwavelength structures; (350.4238) Nanophotonics and photonic crystals; (050.2230) Fabry-Perot; (250.5230) Photoluminescence.

References and links

1. E. Yablonovitch and G. D. Cody, "Intensity enhancement in textured optical sheets for solar cells," IEEE Trans. Electron Dev. **29**(2), 300–305 (1982).
2. A. Goetzberger, "Optical confinement in thin Si solar cells by diffuse back reflectors", in 15th Photovoltaic Specialists Conference, Kissimmee, FL (1981).
3. S. Mokkapati and K. R. Catchpole, "Nanophotonic light trapping solar cells," J. Appl. Phys. **112**(10), 101101 (2012).
4. L. Zeng, Y. Yi, C. Hong, J. Liu, N. Feng, X. Duan, L. C. Kimerling, and B. A. Alamariu, "Efficiency enhancement in Si solar cells by textured photonic crystal back reflector," Appl. Phys. Lett. **89**(11), 111111 (2006).
5. H. Sai, H. Fujiwara, M. Kondo, and Y. Kanamori, "Enhancement of light trapping in thin-film hydrogenated microcrystalline Si solar cells using back reflectors with self-ordered dimple pattern," Appl. Phys. Lett. **93**(14), 143501 (2008).
6. Z. Yu, A. Raman, and S. Fan, "Fundamental limit of light trapping in grating structures," Opt. Express **18**(S3 Suppl 3), A366–A380 (2010).
7. E. Garnett and P. Yang, "Light Trapping in Silicon Nanowire Solar Cells," Nano Lett. **10**(3), 1082–1087 (2010).
8. J. Wallentin, N. Anttu, D. Asoli, M. Huffman, I. Aberg, M. H. Magnusson, G. Siefer, P. Fuss-Kailuweit, F. Dimroth, B. Witzigmann, H. Q. Xu, L. Samuelson, K. Deppert, and M. T. Borgström, "InP Nanowire Array Solar Cells Achieving 13.8% Efficiency by Exceeding the Ray Optics Limit," Science **339**(6123), 1057–1060 (2013).
9. K. Q. Peng and S. T. Lee, "Silicon Nanowires for Photovoltaic Solar Energy Conversion," Adv. Mater. **23**(2), 198–215 (2011).
10. J. Kupec, R. L. Stoop, and B. Witzigmann, "Light absorption and emission in nanowire array solar cells," Opt. Express **18**(26), 27589–27605 (2010).
11. M. Law, L. E. Greene, J. C. Johnson, R. Saykally, and P. Yang, "Nanowire dye-sensitized solar cells," Nat. Mater. **4**(6), 455–459 (2005).
12. H. A. Atwater and A. Polman, "Plasmonics for improved photovoltaic devices," Nat. Mater. **9**(3), 205–213 (2010).
13. S. Pillai and M. A. Green, "Plasmonics for photovoltaic applications," Sol. Energy Mater. Sol. Cells **94**(9), 1481–1486 (2010).

#328692 https://doi.org/10.1364/OE.26.00A806
Journal © 2018 Received 27 Apr 2018; revised 28 Jun 2018; accepted 9 Jul 2018; published 26 Jul 2018

Optics EXPRESS

14. V. E. Ferry, M. A. Verschuuren, H. B. T. Li, E. Verhagen, R. J. Walters, R. E. I. Schropp, H. A. Atwater, and A. Polman, "Light trapping in ultrathin plasmonic solar cells," Opt. Express **18**(S2), A237–A245 (2010).
15. A. Cattoni, P. Ghenuche, A.-M. Haghiri-Gosnet, D. Decanini, J. Chen, J.-L. Pelouard, and S. Collin, "λ^3/1000 Plasmonic Nanocavities for Biosensing Fabricated by Soft UV Nanoimprint Lithography," Nano Lett. **11**(9), 3557–3563 (2011).
16. Q. Gan, F. J. Bartoli, and Z. H. Kafafi, "Plasmonic-Enhanced Organic Photovoltaics: Breaking the 10% Efficiency Barrier," Adv. Mater. **25**(17), 2385–2396 (2013).
17. L. Novotny and N. van Hulst, "Antennas for light," Nat. Photonics **5**(2), 83–90 (2011).
18. K. Söderström, F.-J. Haug, J. Escarré, O. Cubero, and C. Ballif, "Photocurrent increase in n-i-p thin film silicon solar cells by guided mode excitation via grating coupler," Appl. Phys. Lett. **96**(21), 213508 (2010).
19. I. Massiot, C. Colin, N. Pere-Laperne, P. Roca i Cabarrocas, C. Sauvan, P. Lalanne, J.-L. Pelouard, and S. Collin, "Nanopatterned front contact for broadband absorption in ultra-thin amorphous silicon solar cells," Appl. Phys. Lett. **101**(16), 163901 (2012).
20. I. Massiot, C. Colin, C. Sauvan, P. Lalanne, P. R. Cabarrocas, J. L. Pelouard, and S. Collin, "Multi-resonant absorption in ultra-thin silicon solar cells with metallic nanowires," Opt. Express **21**(S3), A372–A381 (2013).
21. I. Massiot, N. Vandamme, N. Bardou, C. Dupuis, A. Lemaître, J.-F. Guillemoles, and S. Collin, "Metal Nanogrid for Broadband Multiresonant Light-Harvesting in Ultrathin GaAs Layers," ACS Photonics **1**(9), 878–884 (2014).
22. L. Pronneke, G. C. Glaeser, and U. Rau, "Simulations of geometry effects and loss mechanisms affecting the photon collection in photovoltaic fluorescent collectors," EPJ Photovoltaics **3**, 30101–30111 (2012).
23. L. H. Slooff, E. E. Bende, A. R. Burgers, T. Budel, M. Pravettoni, R. P. Kenny, E. D. Dunlop, and A. Buechtemann, "A luminescent solar concentrator with 7.1% power conversion efficiency," Phys. Status Solidi Rapid Res. Lett. **2**(6), 257–259 (2008).
24. F. Pardo, P. Bouchon, R. Haïdar, and J.-L. Pelouard, "Light funneling mechanism explained by magnetoelectric interference," Phys. Rev. Lett. **107**(9), 093902 (2011).
25. H. C. Casey, and E. Buehler, "Evidence for low surface recombination velocity on n-type InP," Appl. Phys. Lett. **30**(5), 247–249 (1977).
26. Y. Rosenwaks, Y. Shapira, and D. Huppert, "Evidence for low intrinsic surface-recombination velocity on p-type InP," Phys. Rev. B Condens. Matter **44**(23), 13097–13100 (1991).
27. B. Portier, F. Pardo, P. Bouchon, R. Haïdar, and J.-L. Pelouard, "Fast modal method for crossed grating computation, combining finite formulation of Maxwell equations with polynomial approximated constitutive relations," J. Opt. Soc. Am. A **30**(4), 573–581 (2013).
28. E. Palik, *Handbook of Optical Constants of Solids* (Academic, 1985).
29. C. J. Keavney, V. E. Haven, and S. M. Vernon, "Emitter structures in MOCVD InP solar cells", Conference Record *21th IEEE Photovoltaic Specialists Conference*, Kissimmee 141–144 (1990).
30. W. G. J. H. M. van Sark, K. W. J. Barnham, L. H. Slooff, A. J. Chatten, A. Büchtemann, A. Meyer, S. J. McCormack, R. Koole, D. J. Farrell, R. Bose, E. E. Bende, A. R. Burgers, T. Budel, J. Quilitz, M. Kennedy, T. Meyer, C. M. Donegá, A. Meijerink, and D. Vanmaekelbergh, "Luminescent Solar Concentrators-a review of recent results," Opt. Express **16**(26), 21773–21792 (2008).
31. F. Proise, F. Pardo, S. W. A. Maulidiani, A.-L. Joudrier, C. Dupuis, N. Bardou, J.-F. Guillemoles, and J.-L. Pelouard, "Structured InP-based nanoantenna for photovoltaics applications," Journal of Photonics for Energy **5**(1), 053098 (2015).
32. J.-L. Pelouard, J.-F. Guillemoles, F. Proise, M. Paire, D. Lincot, "Photovoltaic component with high conversion efficiency", Patent n° WO2014049157A2, (2014).
33. H.-J. Song, B. G. Jeong, J. Lim, D. C. Lee, W. K. Bae, and V. I. Klimov, "Performance limits of Luminescent Solar Concentrators tested with seed/quantum-well quantum dots in a selective-reflector-based optical cavity," Nano Lett. **18**(1), 395–404 (2018).
34. F. Proise, "Study and realization of micro/nano photovoltaic cells and their concentration system", PhD Thesis, UPMC 2014, *https://tel.archives-ouvertes.fr/tel-01137589/document*
35. D. A. Goldman, J. Murray, and J. N. Munday, "Nanophotonic resonators for InP solar cells," Opt. Express **24**(10), A925–A934 (2016), doi:10.1364/OE.24.00A925.
36. R. D. Needell, O. Ilic, C. R. Bukowsky, Z. Nett, L. Xu, J. He, H. Bauser, B. G. Lee, J. F. Geisz, R. G. Nuzzo, A. P. Alivisatos, and H. A. Atwater, "Micro-optical Tandem Luminescent Solar Concentrators", (2017), arXiv:1710.00034.
37. J. Wong, D. Jariwala, G. Tagliabue, K. Tat, A. R. Davoyan, M. C. Sherrott, and H. A. Atwater, "High Photovoltaic Quantum Efficiency in Ultrathin van der Waals Heterostructures," ACS Nano **11**(7), 7230–7240 (2017), doi:10.1021/acsnano.7b03148.
38. A. Cattoni, H. Chen, J. Goffard, R. De Lépinau, B. Behaghel, C. Dupuis, N. Bardou, and S. Collin, "Multiresonant light trapping in ultra-thin GaAs and CIGS solar cells," in Light, Energy and the Environment, OSA Technical Digest (online) (2017), paper PW3A.2.
39. A. F. Koenderink, A. Alù, and A. Polman, "Nanophotonics: Shrinking light-based technology," Science **348**(6234), 516–521 (2015).
40. R. Saive and H. A. Atwater, "Mesoscale trumps nanoscale: metallic mesoscale contact morphology for improved light trapping, optical absorption and grid conductance in silicon solar cells," Opt. Express **26**(6), A275–A282 (2018).

Optics EXPRESS

1. Introduction

One main axis of research in photovoltaics is the absorber volume reduction to drop costs and absorber material consumption, both issues of increasing importance as photovoltaic industry develops towards the TW scale. It explains the appearance of a second photovoltaic generation with highly absorbing materials (CdTe, $Cu(In,Ga)Se_2$), allowing two orders of magnitude thickness reduction compared to classical 200 µm thick c-Si. Pioneered by Yablonovitch [1] and Goetzberger [2], conventional Lambertian back reflector can be used to increase light pathway. While optical absorption enhancement can be as high as $4n^2$ (n is the medium refractive index), it requires surface roughness larger than the wavelength, which is incompatible with sub-wavelength size [12,14,15,39]. More recently, efforts have been focused to push absorber volume downwards to reach sub-wavelength dimensions [39,38], down to nanometer scale and 2D materials [37], while at the same time considering conditions for electrical collection of photo-generated carriers [40]. At this scale, finding a highly absorbing material is not enough to circumvent loss absorption, which leads to consider advanced light trapping strategies. Three main alternative methods have been proposed. One of them is back reflector gratings, allowing the incident wave to couple to numerous propagating diffraction modes inside the absorbing layer [3–5]. Another method is light trapping enhancement which can exceed $4n^2$ but is strongly angle dependent [6]. Due to technological progress in nano-fabrication during the last decades, in terms of control of features at subwavelength scales implemented on various materials, of devices based on light trapping in standard p/n diodes, as, e.g. based on InP with improvements above that of standard antireflection coatings [35] or in nanowires of various sorts were proposed by several research groups. For example, silicon nanowires with p-n radial junction [7,9], InP nanowire array [8,10], or nanowire based dye-sensitized solar cell [11]. The third strategy, developed in this work, is based on nano-resonators to confine the electro-magnetic field in small volumes [12–17]. In photovoltaics, nano-photonic light trapping has been applied to low absorbing material, such as inorganic or a-Si solar cells [14,18–20]. References [19] and [20] have reported almost 70% optical efficiency on 90 nm thick a-Si solar cell at normal incidence using mainly Fabry-Perot resonances. In this paper, optical efficiency is the percentage of AM 1.5 photons below the bandgap that are absorbed by the photovoltaic cell. More recently, Massiot *et al*. [21] reported 67% optical absorption in 25 nm thick GaAs-based device. While impressive from the optical point of view, 25 nm thick absorber may be too thin from the electrical point of view to include a p/n diode allowing for the efficient extraction of photo-carriers. If this point is considered, we note that in addition to reduce the absorber volume, ultra-thin absorber could improve charge collection by minimizing the photo-carrier recombination in the volume of the absorber.

All the previously cited structures are multi-resonant, which means that they exhibit multiple, spectrally-thin, resonances to harvest the broad-band solar spectrum. One of the challenges lies in designing the device in a way that resonances homogeneously cover the solar spectrum. This can be achieved by combining several resonance mechanisms in the same device or use multiple orders of a single mechanism. While efficient, this approach makes the resonator design difficult, especially with small bandgap semiconductors that require absorption enhancement over a large photon energy spectrum. In this paper, we propose an innovative approach which consists in narrowing the solar spectrum with a spectral convertor made of dye-doped matrix to match a thin spectral bandwidth resonance. This approach comes down to simplify the resonator design, transferring the difficulty to the less challenging spectral convertor, following the geometrical optics regime. Thus, optical efficiency is maximized and the absorber volume is minimized, while being still electrically compatible. Devices known as luminescent solar concentrators have been studied in the literature but their performances are low due to their high sensitivity to non-ideal parameters [22, 23]. Although we take advantage of part of the luminescent solar concentrators concept [33] (spectral conversion), the approach studied here does not incur all its losses.

Optics EXPRESS

Nevertheless, this system can also be coupled to polymer luminescent sheet concentrators and yield very high power relative to active photovoltaic material and systems that could be easily integrated in devices or buildings, a topic that has recently attracted considerable attraction (e.g [33]. and refs therein) and may continue to do so as luminescence quantum yield approaching 100% are demonstrated using quantum dots [33, 36]. After describing the modeling, we show how the device has been designed to perform optimally. Despite low absorber volume, optical efficiency up to 66.2% can be theoretically achieved. The above mentioned result takes into consideration light polarization and spectral distribution, angular dependency and loss mechanisms in both optical stages. In a second phase, we analyze the reasons behind this result using a top-down approach. First the nano-resonator absorption spectrum and electric field map are shown, followed by the angular dependency. Then we endeavor to highlight the benefits of the spectral convertor / nano-resonator coupling. Finally, considerations on the dye feature are given.

2. Method

2.1 Device structure

We consider a 1D nano-resonator embedded in a spectral convertor (Fig. 1). The photoactive layer is a pin junction (thickness t) of absorbing semiconductor bordered with two metal reflecting layers (thickness t_m for the top metal, considered infinite at the back). Apart from the back mirror, all the layers are structured (width w, period p). Our strategy to develop nano-resonator in which even the semiconductor is structured relies on the so-called funneling effect [24]. It allows lateral concentration because the nano-antenna optical cross section is larger than its area. Structuring also generates semiconductor / air interfaces, which can lead to increase recombination and ultimately a loss on the open-circuit voltage. InP was selected as absorber because it has low surface recombination velocity [25, 26] and a direct bandgap at 1.34 eV, well matched to the solar spectrum. Silver is the best performing metal at visible wavelengths and was selected for the metallic reflectors. The spectral convertor (thickness t_c) is made of a PolyMethyl MethAcrylate (PMMA) doped with a dye. PMMA is a suitable material for this application because of its high transparency in the visible, stability and doping-facility. We choose a dye absorption and emission spectrum corresponding to a commercially available dye Lumogen RED 305, shifted of 0.35 eV towards low energy. The shift allows a better matching between the dye emission spectrum and the InP bandgap, thus being a good trade-off between real and perfectly matched dye. The shift value has been optimized (not shown here) to obtain a good match between InP bandgap and dye emission spectrum and to reduce photons number emitted below InP bandgap.

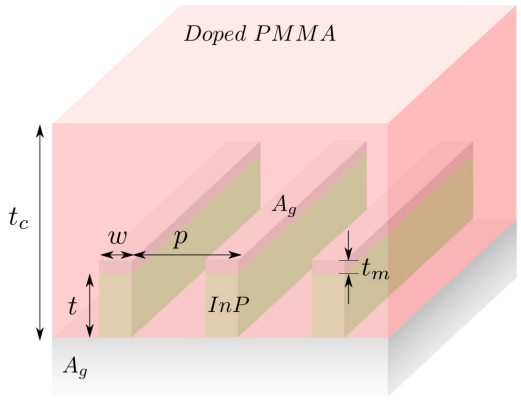

Fig. 1. Schematic of a nano-antenna array and its spectral convertor. The back silver layer supports a structured (width w, period p) InP pin junction (thickness t) and a top silver layer (thickness t_m), embedded in a doped PMMA cavity (thickness t_c).

Optics EXPRESS

2.2 Modeling

The system modeling is a multiscale problem since it involves both sub-wavelength optics for nano-resonator and geometrical optics with a Monte Carlo algorithm for the (thick) spectral convertor. The nano-resonator array optical response is modeled by a Rigorous Maxwell Constitutive Approximation code (RMCA [27]), a 1D electromagnetic solver based on modal approach. To couple the spectral convertor (modeled with incoherent light) to the nano-resonator array (modeled with Maxwell's equations), we assumed that absorption in the nano-resonator could be well approximated by averaging polarizations and directions of light at each wavelength as given by the Monte-Carlo algorithm and using the detailed response at each polarization, wavelength and direction as computed by the RMCA code.

This is justified in the cases of interest, where the fluorophore has a high quantum yield, so that it can be used at concentrations high enough for complete absorption of the solar spectrum in its absorption band, and where the nano-resonator array is well matched to the emission band of the fluorophore, for all directions (Fig. 8): then, irrespective of the incidence of the nano-resonator, the light is absorbed by the device. Moreover, because the spectral convertor is thick (mm), minute variations of thickness would destroy interference effects. This eliminates correlations that might be due to reflections on the nano-resonator bouncing back on the array after scattering in the spectral convertor and would not be accurately treated by the Ray tracing code.

The refractive indices of silver and InP are taken from the Palik database [28] and PMMA refractive index is set at 1.5. RMCA calculates the absorptivity in each layer for each incidence angle (θ_i), wavelength (λ) and polarization. Sun light is not polarized and we assume that light emitted by the dye is not polarized. Unpolarized values are obtained by taking the arithmetic mean over TE and TM polarization. From these absorptions, we deduce the absorption in the photoactive layer $A_{photo}(\theta,\lambda)$, the parasitic absorption $A_{loss}(\theta,\lambda)$ (in metal layers) and the reflectivity $R(\theta,\lambda)=1-A_{photo}(\theta,\lambda)-A_{loss}(\theta,\lambda)$. Since the spectral convertor follows geometrical optics, it is modeled with a home-made ray-tracing code based on a Monte Carlo algorithm, using periodic lateral boundary conditions [34]. When a photon hits the spectral convertor back surface (i.e. hits the nano-resonator array), the outcome is determined by testing a random number (uniform distribution on the interval [0 1]) against A_{photo}, A_{loss} and R parameters corresponding to the photon wavelength and incidence angle. For calculation speed sake, four θ values are considered (0°, 20°, 40° and 60°). Using fewer angles was found too rough an approximation.

We neglect electron-hole pair recombination in the ultra-thin pin junction doped layers (typically 10 nm thick), therefore we consider the whole pin junction as photoactive. This assumption will be discussed in section 3.3. We consider the PMMA cavity thickness t_c = 2 mm and top metal thickness t_m = 15 nm. Dye concentration is 250 ppm and its photoluminescence quantum yield is assumed ideal. These parameters influence on the whole device will be discussed in section 3.2.

3. Results

In this section we describe how a nano-resonator array can be designed to perform optimally and we analyze its optical performances.

3.1 Design

The optimization of geometrical parameters allows a better light confinement by giving rise to resonances adapted to the dye emission spectrum. To do so, we vary simultaneously the period p, width w and InP thickness t. We also define in Eq. (1) the mean thickness t_{mean} which represents the averaged InP thickness per unit area:

Optics EXPRESS

$$t_{mean} = \frac{w}{p}.t \quad (1)$$

Geometrical parameters used for the nano-resonator design are summarized in Table 1.

Table 1. Geometrical parameters used for nano-resonator optimization

Parameters	Thickness (nm)
Top metal	$t_m = 15$
Pin junction	$t \in$ [70, 120], step = 10 nm
Period	$p \in$ [150, 1000], step = 50 nm
Width	$w \in$ [80, 300], step = 20 nm
Mean thickness	$t_{mean} \in$ [5.6 - 104]

Since we seek to reduce t as much as possible, we restrict ourselves to $t \in$ [70 – 120] nm. The lower limit of 70 nm is chosen to avoid situation where device design (that should account for a p/n junction for selective extraction of electron and holes, as well as for electrically passivating contacts) becomes not realistic with current technologies. We limit the width to 80 nm because of fabrication issue. Results are shown in Fig. 2.

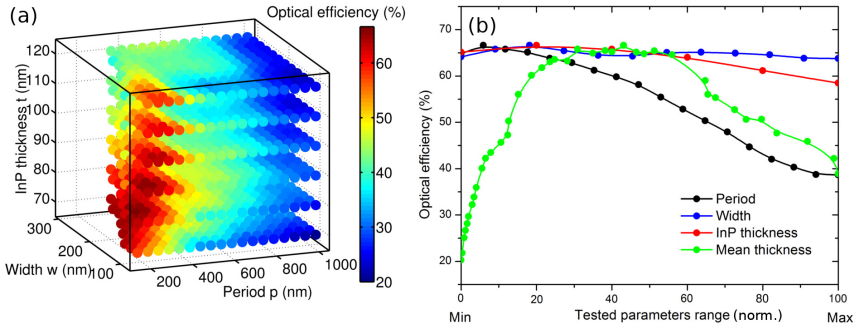

Fig. 2. Nano-resonator design. (a) Optical efficiency (colormap) as a function of t, w and p. (b) Best optical efficiencies for each parameter. x-axis is standardized. As an example, for the black curve corresponding to the period, min designates 150 nm whereas max corresponds to 1500 nm (see Table 1 for the tested parameters range). Optical efficiencies standard deviation is 0.15%.

Figure 2(a) shows that there is only one maximum at 66.6% for a mean thickness of 48 nm, corresponding to the triplet $\{p = 200,\ w = 120,\ t = 80$ nm$\}$. The efficient zone (efficiency larger than 60%) is broad, which means we have a certain tolerance on the geometrical parameters, which is precious when one thinks to fabrication. Figure 2(b) highlights the relative influence of the tested parameters. The most critical parameter is the period. The width curve (blue) is almost constant: for any given width, there is always a couple $\{p,t\}$ allowing efficiency larger than 65%. There is an optimal value of InP thickness, but the maximum is flat (red curve). Efficiency larger than 65%, corresponding to 20.1 mA/cm^2, can be achieved for mean thickness ranging from 35 to 60 nm. By comparison, the best InP-based solar cell exhibits 29.5 mA/cm^2 for 3 µm thick InP layer [29]. The maximum optical efficiency region (red / brown area in Fig. 2(a)) is close to the cube borders at low width and period. Yet, complementary calculations (not shown here) for lower period and width have not shown better optical efficiency, which means that the maximum is an optimum. Naturally, this result is strongly dependent on the dye and optical efficiency may be improved with a better dye. This point will be discussed at the end of this paper. Finding analytical relationship between the geometrical parameters to perform optimally seems out of reach due to the complexity of the device. Yet some design trends can be given, as shown in Fig. 3.

Optics EXPRESS

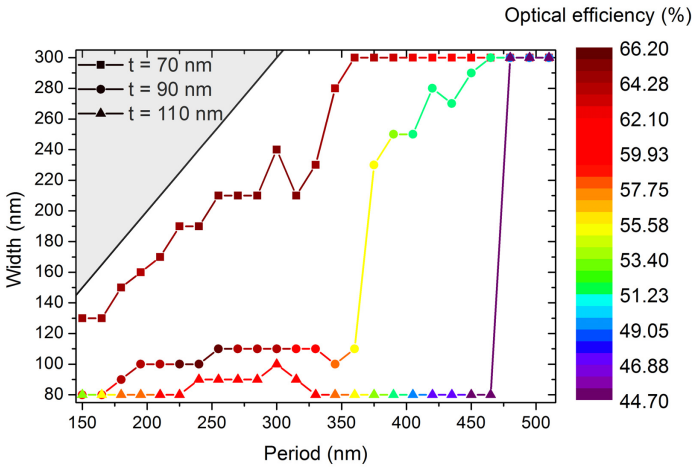

Fig. 3. Design trends. For three different InP thickness t of 70, 90 and 110 nm (squares, circles and triangles respectively), we represent the couple {period, width} allowing the best optical efficiency, given as a colormap. The upper left grey triangle represent non-physical configuration (width cannot be higher than period).

Interestingly, the width is an increasing function of the period. Yet the optimal filling factor w/p differs according to the InP thickness t. Figure 3 exhibits step shape graphs, all the stiffer that the thickness is large. This behavior is due to a saturation effect, especially on the width. At low period, lower width should be considered to avoid saturation. At low thickness, high filling factors are favored and optical efficiency is always higher than 60%. At higher thickness, the transition between low and high width becomes sharper and occurs at larger period. Additionally, tolerance on the optical efficiency is better at low thickness. The meshing calculation has been refined on the efficient zone and we find that the triplet $\{p = 250,\ w = 115,\ t = 87.5\ \text{nm}\}$ reaches 66.2% optical efficiency for a mean thickness of 40 nm. This geometry offers the best trade-off on the ratio efficiency / volume. This is due to the optimized coupling between the antenna and the spectral convertor. The first step of the analysis is to look at the whole device (spectral concentrator and nano-resonator) spectral response, as shown in Fig. 4.

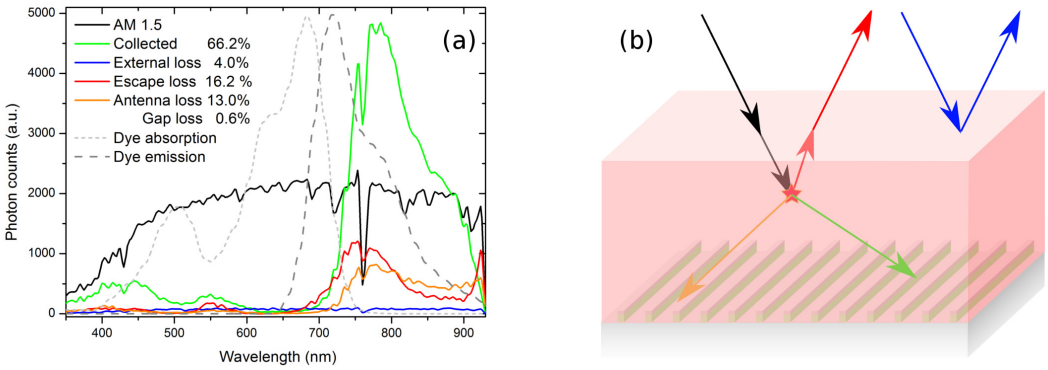

Fig. 4. (a) Spectral output of the optimized structure. Green curve represents the photons which have been absorbed in the InP layer. Blue curve is the Fresnel loss due to the interface air/PMMA. Red curve is the escape loss through the front surface of the spectral convertor. Orange curve represents photons absorbed in the metal layers. Gap loss is not represented since it occurs at wavelength larger than InP bandgap. The normalized absorption and emission spectrum of the dye are also given (dash curves). The red-shift between the emission coefficient and the emitted spectrum is due to dye self-absorption [30]. (b) Scheme of the device. Loss channels are illustrated with colored arrows. Red star represents dye absorption.

Optics EXPRESS

Figure 4 shows that the nano-resonator design adapted to the spectral convertor is efficient, leading to 66.2% of optical efficiency. The two main loss causes are the escape loss (16.2%) and the parasitic absorption in nano-resonator metal layers (13%). Escape loss generally occurs when photon incident angle on the front surface is lower than the critical angle $\theta_c = asin\left(n_{air} / n_{PMMA}\right)$. External loss is only 4% and may be reduced by adding an antireflective coating, whereas gap loss (photon wavelength higher than InP bandgap) is lower than 1%.

3.2 Optimization of the fluorophore utilization

The nano-resonator design is dependent on the spectral convertor. Apart from the matrix refractive index, the dye absorption/emission spectra, concentration and photoluminescence quantum yield are determining. We have presented on Fig. 5 the influence of dye concentration and photoluminescence quantum yield on the optical efficiency. Dye concentration set to zero leads to 57.3% optical efficiency, considering all photons incoming at normal incidence. It can be seen that the dye contributes additional power conversion only if its photoluminescence quantum yield is larger than 72%. The optimal dye concentration is an increasing function of the quantum yield, which is all the sharper than the quantum yield is low. This behavior can be easily understood knowing that increasing the dye concentration has one beneficial effect, obtaining a modified solar spectrum better matched to the nano-resonator, and two drawbacks, increasing escape loss and non-radiative de-excitation. The optimal trade-off is depicted by the black dots in Fig. 5.

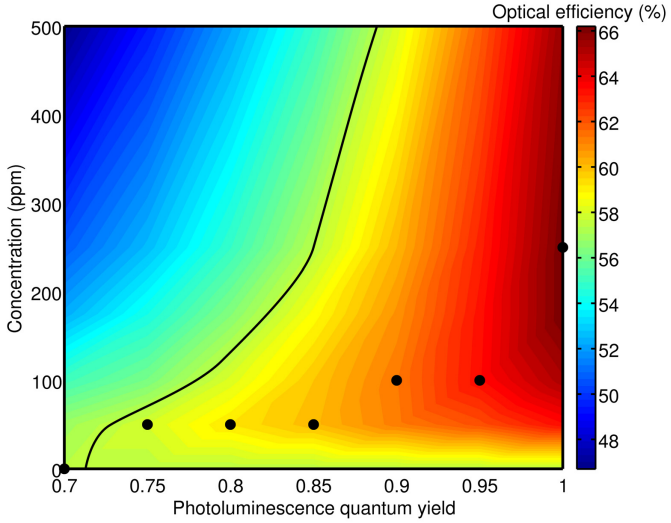

Fig. 5. Effect of the dye concentration and photoluminescence quantum yield on the optical efficiency. The black curve marks out the condition on the concentration and photoluminescence quantum yield where the use of the dye produces no net additional power conversion. The dye should be used only at the right of the black curve. Black dots are a guide for the eyes showing the optimal dye concentration for a given quantum yield.

It is worth noting that a new optimization made without dye leads to a different optimized structure $\{ p = 450 , w = 280 , t = 70$ nm$\}$ with an optical efficiency of 61% (integrated over wavelength, polarization and incidence angle). Even in this case, the use of the dye leads to almost 10% relative enhancement despite additional optical losses due to the escape cone emission. In the best conditions (concentration 250 ppm and quantum yield ideal), the use of the dye allows an enhancement of 9% (absolute) on the optical efficiency. This number depends on the dye emission spectral shape and can be improved with a thinner emission bandwidth.

Optics EXPRESS

3.3 Analysis of the nano-resonator

The optical response of the resonator is shown in Fig. 6.

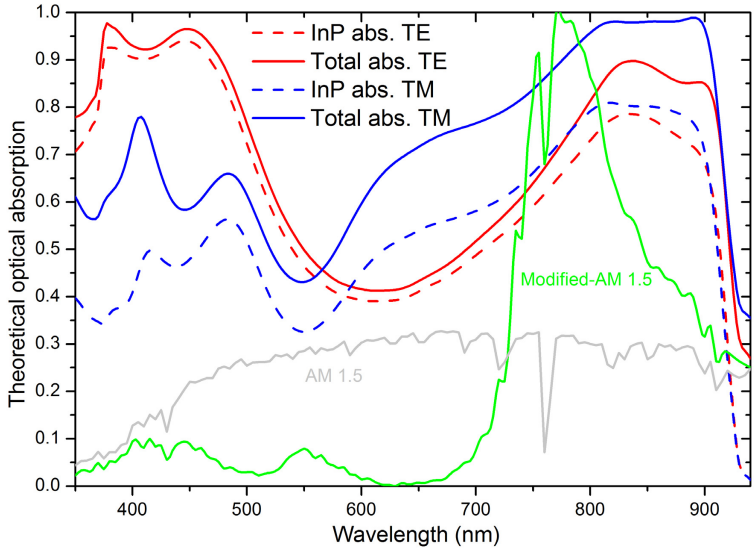

Fig. 6. Total / InP (solid / dash) absorption spectra in TE and TM polarization (red and blue respectively) at normal incidence. AM 1.5 is represented in gray as well as the spectral convertor-modified AM 1.5 in green. It represents the spectrum of the photons reaching the nano-resonator array.

InP absorption is higher at high wavelength, more than 50% on the [700 – 940] nm range. Even though this behavior was predictable, the good response for low wavelengths is unexpected since only 12.2% of photons reach the nano-resonator with a wavelength below 620 nm. That contributes to explain why 57.3% optical efficiency is reached even if the PMMA matrix is not doped. The remarkably good absorption despite low InP volume is mainly due to the strong resonance around 820 nm (835 nm in TE, 810 nm in TM). We stress that absorption in these InP nanostructures can be over 5 times larger than what it would be in a single InP slab of the same average thickness.

Parasitic losses (i.e., metal absorption) are greater in TM than in TE polarization. It can be understood with electric field intensity maps in both polarizations at the resonance, represented in Fig. 7.

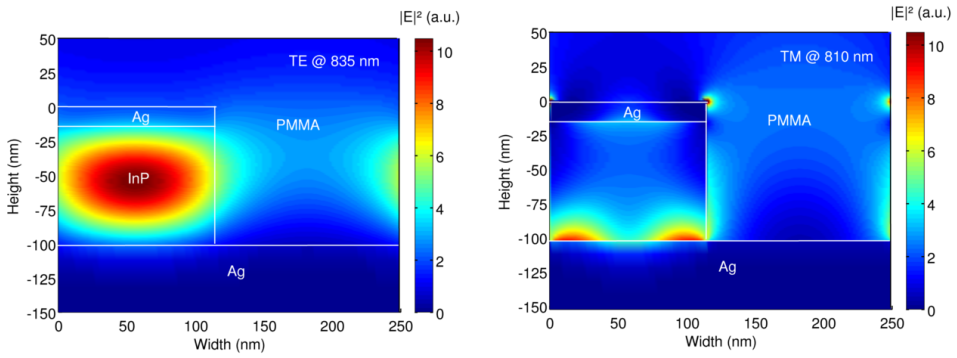

Fig. 7. Electric field intensity ($|E|^2$) map at 835 nm / 810 nm in (TE / TM). Electric field confinement in TE is typical of 1st order Fabry-Perot resonance. In TM, confinement at the interface InP/metal is an evidence of plasmonic resonance.

Optics EXPRESS

Electric field confinement in TE is well centered in the InP photoactive layer, that is why metal absorption is reduced compared to TM in which the electric field intensity is located at the interfaces. In TE, the remarkable confinement in the InP layer is typical of a 1st order Fabry-Perot mechanism, whereas the field enhancement in TM is typical of plasmonic resonance. In TE polarization, heavily InP doped layers (p + and n +) would not be an issue for photo-carriers' recombination since the field enhancement, and therefore the absorption, is far from the interface. On the other hand, in TM, the field enhancement occurs mainly close to the interface. Assuming that absorption in these two layers (10 nm thick each, no optical constant change due to doping) are considered as loss, back loss rises to 28.8% and optical efficiency lowers to 50.4% (calculation not shown). The real back loss is likely to be in-between 13% and 28.8% because the extremely low thickness of doped layers may allow photo-carriers diffusion before recombination. Despite good behavior at normal incidence, the nano-resonator has to be angular tolerant. This is a general issue in photovoltaics since the Sun position is moving across the sky, but in our case, this is even more critical due to isotropic emission pattern of the dye in the spectral convertor. Figure 8 shows the angular tolerance.

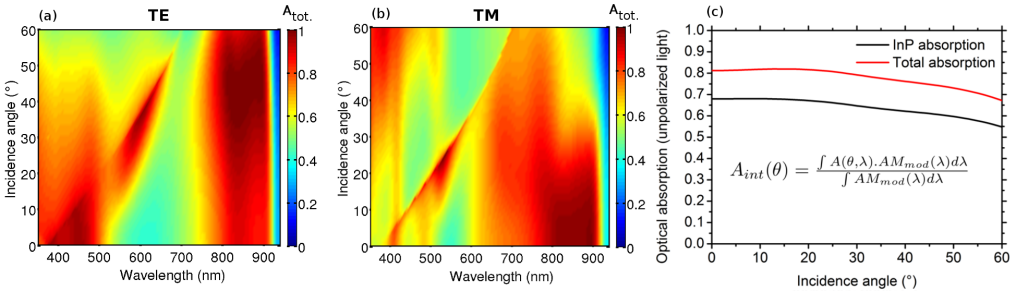

Fig. 8. Tolerance to incidence angle. Total absorption spectrum as a function of the wavelength and the angle of incidence in TE (a) or TM (b) polarization. (c) Integrated optical absorption over the spectral convertor-modified AM 1.5 spectrum (AM_{mod}, obtained from green curve in Fig. 6) as a function of the incidence angle.

Angular tolerance is reflected by the weak incident angle influence on Fabry-Perot resonances occurring above 700 nm. Others mechanisms occur below 700 nm but are not relevant in this study since almost no light reach the nano-resonator at these wavelengths. Total absorption remains higher than 0.8 in TE. TM polarization is more sensitive to the incident angle with total absorption drop to 0.5 at 60°. Since each wavelength has not the same "weight" on the optical efficiency, we have represented on Fig. 8(c) the optical absorption integrated over the modified AM 1.5 spectrum (see green curve in Fig. 6). It can be seen that InP absorption remains stable until 20°, then lowers at a low rate of −0.28% / degree. The good tolerance to incidence angle suggests that our device is well suited for photovoltaics applications.

3.4 Nano-resonator and spectral convertor coupling

The benefits provided by the spectral convertor are double. First it allows to spectrally concentrate light on the main device resonance, around 820 nm. It can be seen on Fig. 6 that resonances at 820 nm and the modified solar spectrum are slightly mismatched. Yet, a better alignment would have led to photons emission below the InP energy bandgap, resulting in an overall optical efficiency drop. Another beneficial effect is the light trapping improvement due to Fresnel reflection at the interface PMMA / air. We have shown that 16.2% of photons are lost by front escape (see Fig. 4). Front escape event may concern two photons families. The first one is photons which never reached to nano-resonator, they have been absorbed by the dye, re-emitted toward the front surface and get escaped. The second family concerns photons which have been reflected by the nano-resonator and finally escape through the front

Optics EXPRESS

surface. The first family is included in escape loss but is not linked with the nano-resonator reflectivity. To determine this contribution, we have run calculation assuming a perfect nano-resonator (A_{InP} = 1, ∀ θ, λ). It turns out that in this case, escape loss is 7.5%. Thus the proportion of photon lost because of the nano-resonator reflection coefficient is only $16.2 - 7.5 = 8.7\%$. This number can be compared with the integrated reflection coefficient of the nano-resonator, displayed on Fig. 9.

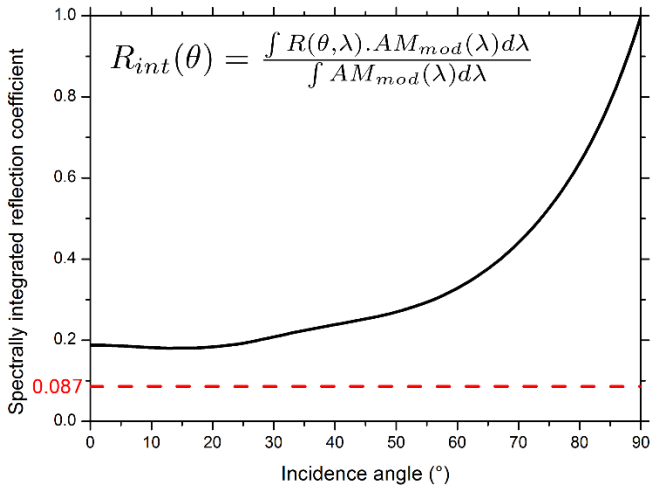

Fig. 9. Photons recycling analysis. Black curve represents the spectrally integrated reflection coefficient of the nano-resonator, derived from the formula given in the graph. AM_{mod} is the solar spectrum reaching the nano-resonator array leaving the spectral convertor (green curve in Fig. 6). Dash red line is a guide for the eyes corresponding to the front loss, due to the nano-resonator reflection coefficient.

Without photon recycling, the front loss due to the nano-resonator reflection coefficient should be higher than the lowest reflection coefficient (≈0.18). This is not the case, which is an evidence of the photon recycling effect due to PMMA / air interface. The two complementary spectral convertor effects of narrowing the solar spectrum and photon recycling contribute to improve optical efficiency if the nano-resonator is adapted. Finally, one can argue about the usefulness of structuring. The same optimization as reported in Table 1 except than InP layer is continuous shows that the best achieved optical efficiency is 66.8% for the triplet $\{p = 300,\ w = 260,\ t = 70$ nm$\}$, with an absorber mean thickness of 70 nm against 40 nm if structured.

4. Conclusion

The aim of this paper was to demonstrate that the coupling between nano solar cells and a spectral conversion may improve the overall device optical efficiency. We have shown that the coupling between a structured nano-resonator array and a spectral convertor theoretically lead to optical efficiency as high as 66.2% with an absorber mean thickness of 40 nm. It is worth noticing that absorption in InP is 5 times larger than what it would be in a single InP slab, while absorber mean thickness is about half the minimum pin junction thickness. Compared to the multi-resonant devices, our approach transfers and reduces the nano-resonator-induced loss to the spectral convertor. Doing so, we take advantage of the spectral conversion and the non-imaging concentration feature of a luminescent solar concentrator as well as almost ideal absorption in a thin spectral region of a nano-resonator array. The good optical efficiency comes from the synergy between the spectral convertor and the nano-resonator array. Although adding the spectral convertor generates intrinsic loss (escape loss due to dye emission), its benefits of narrowing the solar spectrum and improving light

Optics EXPRESS

trapping allow to reach high optical efficiency with low absorber volume. The spectral convertor eases the nano-resonator design since it should be resonant on a thinner spectral bandwidth and also because reflection is not necessarily a loss. Furthermore, the device design is electrically-compatible since the absorber layer is thick enough to hold a pin junction. Structuring InP layer allows to reduce material consumption without reducing the optical efficiency. This work has been done with InP as absorbing material because of its direct bandgap at 1.34 eV and its low surface recombination velocity. Yet this device architecture could be extrapolated to other absorber materials such as GaAs or a-Si, provided that surface recombination is kept low. Prototypes are under development and fabrication process is at an advanced stage [31,32]. Finally, it appears that further improvement relies on the dye's spectral properties optimization. A thinner emission bandwidth shifted to larger wavelength (near infrared) would allow a better matching with the absorber material as well as a thinner modified solar spectrum, reinforcing the coupling between the nano-resonator and the spectral convertor. This improvement must not damage the photoluminescence quantum yield, which tends to indicate that quantum-dots may be a promising alternative to organic dye for this concept.

Funding

"Action Energy" of CNRS.

Acknowledgments

The authors would like to thank Gary Wolfowicz for helping to vectorize the Monte-Carlo algorithm. This work has been supported by "Action Energy" of CNRS.